Surface & Coatings Technology 383 (2020) 125226

Contents lists available at ScienceDirect

Surface & Coatings Technology

journal homepage: www.elsevier.com/locate/surfcoat

Nanostructured titanium alloy surfaces for enhanced osteoblast response: A combination of morphology and chemistry

André L.R. Rangel[a], Céline Falentin-Daudré[b], Bruna Natália Alves da Silva Pimentel[c], Carlos Eduardo Vergani[c], Véronique Migonney[b], Ana P.R. Alves Claro[a,*]

[a] UNESP–São Paulo State University, School of Engineering, Materials and Technology Department, Guaratinguetá Campus, SP, Brazil
[b] Université Paris 13, CSPBAT-LBPS, Paris, France
[c] UNESP – São Paulo State University, Dental School, Dental and Prosthodontics Department, Araraquara Campus, SP, Brazil

ARTICLE INFO

Keywords:
Titanium alloys
Coating
TiO_2 nanotubes
Polymer grafting

ABSTRACT

This study is part of a new trend in the metallic biomaterials field that searches to use the titanium beta alloys with recognized bulk and surface properties for better biological response. Ti15Mo alloy (wt%) had it surface modified by TiO_2 nanotubes growth using the anodic oxidation method and grafted with poly(sodium styrene sulfonate) (PNaSS). The motivation behind the combination of these techniques was to promote a surface, which enables better osteointegration associated with antimicrobial behavior. Surfaces were characterized and subjected to cell culture assays and bacterial colonization to evaluate their *in vitro* response. The results showed that the surfaces were completely covered with TiO_2 nanotubes, which was successfully grafted with PNaSS. Compared with untreated Ti 15Mo surfaces, PNaSS grafted nanotubes surfaces showed better osteoblast cell response in terms of cell attachment and mineralization and weaker bacterial adhesion and colonization. The results suggest that the final product of the combine treatment – nanotube plus PNaSS grafting - represents a promising option to improve commercial metallic implants.

1. Introduction

The use of titanium-based metal alloys as a substitute or reinforcement of biological hard tissues has become commonplace in our society due to their favorable mechanical characteristics and bioinertness. Although essential for early success of these materials in biomedical application, these properties are no longer sufficient to the accomplishment of an implanted material.

When a material is inserted into the human body, a series of cascade reactions occurs, which can lead to its integration. The first step in this process is called primary stability and is related to implant anchorage to the bone, but over time, this relationship loses importance to the detriment of a second stage, the biological connection between the involved parts [1]. This process suggests that factors as topology, roughness and surface composition, play a major role for a favorable outcome. All these characteristics could be connected, since surface structure and roughness are prime parameters for wettability profile, which will change the way that bone cells proliferate across the surface. Furthermore, cell differentiation is closely linked to surface composition [2] and its growth will mainly occur in gaps left by roughness [3]. Following this premise, surface modification techniques have been proposed in the past, acting over surface morphology, chemistry or both.

Nanostructured surfaces resemble the extracellular matrix structure and this morphology favors cell adhesion in a direct and indirect manner [4–6]. Anodization can be used to obtain TiO_2 nanotubes on titanium alloys surface and it is important to emphasize that the morphology of the nanotubes, such as length, diameter and/or wall thickness, plays a fundamental role in the stabilization of the constituent phase of titanium dioxide [7,8], which can also influence cell growth.

The growth and proliferation of osteoblast cells on anodized surface of commercially pure titanium were studied by different authors and the results regarding the number of adhered cells were promising even in short time interval [9]. The increment can reach more than 300% [10] and is mainly attributed to the topography of the surface since besides providing a substantial increase of the surface area it also presents favorable morphology for the cellular anchorage [11].

Although the topography of surfaces treated by anodic oxidation is favorable to osteointegration, chemically the nanotubes still consist of the same inert titanium dioxide found in compact layers. Moreover, pores created on the surface may also represent a locus for bacterial accumulation [12] and thus, additional treatments can complement

* Corresponding author.
E-mail address: paula.rosifini@unesp.br (A.P.R. Alves Claro).

https://doi.org/10.1016/j.surfcoat.2019.125226
Received 4 October 2019; Received in revised form 29 November 2019; Accepted 3 December 2019
Available online 16 December 2019

beneficial effect of nanotubes on cells [13], for example the surface functionalization by bioactive polymer grafting.

This method has gained prominence in the recent years due to the possibility of modify implant surfaces aiming to the improvement of cell adhesion by immobilization of extracellular proteins [14,15]. For instance, grafting poly(sodium styrene sulfonate) (PNaSS) creates surfaces rich in negative ionic groups, which would act as active sites for the interactions with binding proteins such as fibronectin or bone growth factors [16].

In addition to improving *in vitro* calcium-phosphate deposition [17,18] and *in vivo* bone formation [19,20], such treatment can play an inhibitory role on bacterial adhesion for both gram positive and negative strains [21,22]. It was found that the adhesion of bacteria to pNaSS grafted surfaces in the presence of pure or diluted blood plasma and of different protein solutions are strongly influenced by the presence of sulfonate groups in the macromolecular chains of the grafted polymer [23].

This combination of bacterial adhesion inhibiting effect and ability to improve osteointegration in a single treatment is rare and makes PNaSS grafting an advantageous procedure and excellent candidate to enhance biological responses of nanostructured surfaces.

2. Materials and methods

2.1. Alloy processing

Ti15Mo alloy ingots were obtained from commercially pure titanium and molybdenum plates. Initially the materials were cut and chemically etched in acid solution (HF/HNO_3 1:3 v/v) for 10 s, then washed under running water. The plates were melted in an electric arc furnace and subjected to homogenization heat treatment in tubular furnace at 900 °C for 24 h with slow cooling. The ingots were forged using for cold rotary forging machine to obtain cylinders with 10 mm of diameter. After forging, the alloy was subjected to solubilization heat treatment at 900 °C for 1 h and cooled rapidly in cold water. Both casting and heat treatments were performed under argon atmosphere to avoid oxidation. The bars were cut in discs of 3 mm thickness using a precision cutter. The discs were ground with increasing grit sandpaper (200, 400, 600, 1000, 1200 and 1500, 2000) and rotary polished using colloidal silica (10 μm, OP-U Struers) until mirror-like surfaces were obtained.

2.2. Anodic oxidation

TiO_2 nanotubes were obtained by anodic oxidation using a classic electrolytic cell. Briefly, two electrodes, one inert platinum electrode and the sample to be anodized, were immersed into electrolyte. To prepare the electrolyte, 2.5 g of ammonium fluoride were dissolved in 100 ml of distilled water and this solution was added to 900 ml of glycerol. The solution was homogenized for 5 min. For each sample 100 ml of electrolyte was used, and the assembly was connected to a voltage source. The voltage was raised from 1 V/min until 10 V and kept for 24 h. After treatment the samples were washed in ultrasonic bath for 5 min and annealed at 450 °C in order to crystalize the nanotubes.

2.3. PNaSS grafting

The NaSS grafting was performed based in the protocol established by Falentin-Daudré et al. [24]. The samples were placed in a round bottom flask containing NaSS solution in distilled water (0.7 mol/l) and degassed by argon insertion of argon for 30 min. Subsequently, the flask was subjected to UV radiation (365 nm) for 1 h at 170 mW/cm^2, at room temperature. The Fig. 1 illustrates the scheme of direct UV grafting. The peroxide groups present on the nanotubes layer [25] are decomposed by the action of UV radiation, creating the reactive sites

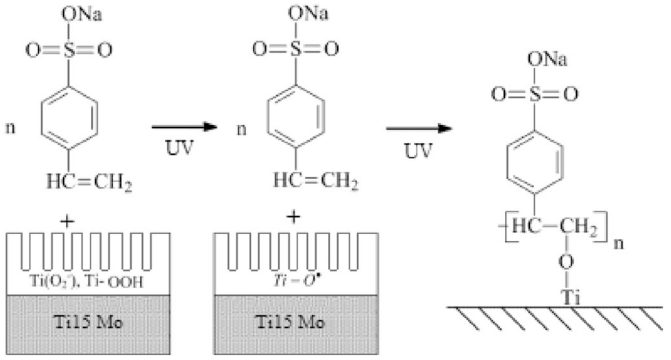

Fig. 1. Model of UV grafting over nanotubes. The grafting sites are created by homolytic fission of peroxides bond.

for covalent grafting [26]. After grafting, the samples were washed in distilled water, renewed four times a day, for 48 h.

2.4. Surface characterization

In order to verify the formation and distribution of the nanotubes on the treated surfaces the samples were investigated by scanning electron microscopy (Philips XL-30 FEG). The dimensions of the nanotubes were measured with the help of the open access software ImageJ.

The change in wettability after surface treatment was analyzed by measuring the contact angle. For each measurement, 200 μl of distilled water were dropped onto the surface. The measurements were made using DAS10 goniometer from Kruss. The drop was deposited over the surfaces and a single image of the drop was taken 20 s after contact. The contact angle was measured by the software from these images. In addition, the polymer-grafted samples were evaluated by Fourier-transformed infrared spectroscopy, in attenuated total reflectance mode (Perkin-Elmer Spectrum two). The spectra were acquired between 4000 and 600 cm^{-1}.

Finally, the quantification of PNaSS grafted was carried out by toluidine blue O (TB) colorimetry assay according to the protocol established by Helary et al. [27]. Briefly, this technique is based on the chemical affinity between pNaSS and toluidine blue. After immersion in dye solution (0.5 mmol/l), the samples are stirred for 6 h at 30 °C for complexation. During this time each mole of polymer combines with 1 mol of dye, which can be recovered after washing in NaOH (10^{-3} mol/l, three times 5 min) and incubation for 24 h in acetic acid solution 50% in distilled water. The concentration of TB in the solution recovered after decomplexing was quantified by UV–visible spectroscopy at 630 nm (PerkinElmer lambda 25 spectrometer).

2.5. Cells culture assays

The treated surfaces were evaluated for cell adhesion, proliferation, morphology, viability and differentiation using MC3T3-E1 osteoblast cells.

The short-term cell adhesion test was performed 15 min after cell seeding and in the adhesion strength test the surfaces were submitted to a shear stress of 10 dyn/cm^2 on the surface for the same time. The intensity of adhesion between cells and the surface can be indirectly measured by the percentage of cells adhered to at the end of the experiment and is expressed in percentage of seeded cells.

The cells morphology at 24 h was observed using environmental scanning electron microscopy images (ESEM - Hitachi TM3000). For cells fixation the samples were taken from the culture medium, washed twice in PBS and immersed in 4% formaldehyde solution for 30 min at room temperature.

The viability of osteoblast was evaluated by MTT assay after 24 h of incubation and the cell proliferation was evaluated by cells counting

(Multisizer III - Coulter Counter Z2 Beckman) after 1, 3 and 7 days of culture.

The differentiation of MC3T3-E1 cells were evaluated by measuring the alkaline phosphatase activity, after 14 and 21 days of culture and mineralization (calcium phosphate deposit) after 21 and 28 days of culture.

2.6. Bacterial colonization assay

The bacterial colonization was evaluated by live/dead assay in confocal microscopy. Samples were exposed to strains of *Staphylococcus aureus* (ATCC 25923) and *Candida albicans* (SC 5314) for 90 min and incubated for 48 h before staining (LIVE/DEAD BacLight Bacterial Viability Kit, Life Technology, Thermo Fischer, Waltham, MA, USA).

3. Results and discussion

3.1. Surface characterization

The morphology of TiO_2 nanotubes after 24 h of anodization was evaluated by scanning electron microscopy. All surfaces were calcined at 450 °C for 1 h after anodic oxidation. Fig. 2(a) shows the top morphology of the nanotubes.

The images show homogeneous formation of TiO_2 nanotubes over the entire surface. Images with higher magnification, as shown in Fig. 2b, were analyzed using ImageJ. The dimensions of the nanotubes were reproducible throughout the samples for both diameters (22.15 ± 2.88 nm) and wall thickness (11.64 ± 1.46 nm). These results agree with previously found for anodized alloys of TiMo system [8,28] and prove the treatment efficiency in the alteration of surface topography.

Thereafter, the samples were subjected to UV irradiation and the grafting degree was evaluated by toluidine blue O (TB) colorimetry assay (Fig. 3).

In this test, flat TiMo (group A) and anodized non-grafted samples (group B) were used as a control to measure the non-specific absorption of the dye on the surfaces. For the group A, such absorption represents no significant values (< 1 nmol), however the same cannot be considered for group B. The values obtained have been much more expressive, however it does not exceed half the value obtained for grafted samples (group C). The non-specific absorption of TB by nanotubes has not been investigated in the literature yet, but all evidence suggests that this fact is mainly due to the higher specific area of nanotubes compared to flat samples, allowing greater interaction. In all cases, the mean difference between only anodized samples and grafted samples

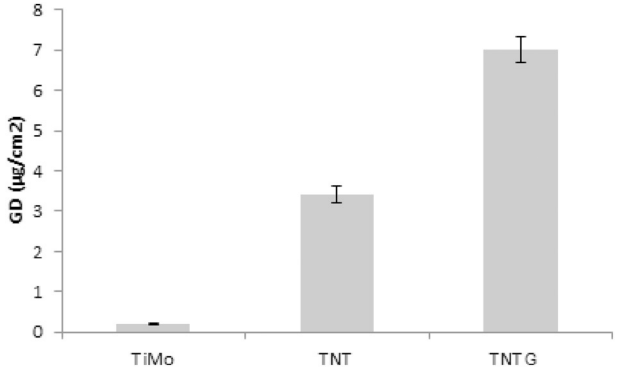

Fig. 3. Grafting degree (µg per effective area): flat samples (TiMo), anodized non-grafted samples (TNT) and anodized and grafted samples (TNT + G).

were greater than 3.5 µg/cm^2 of effective sample area, higher values than previously found for similar procedures in polished alloys [23,25]. Once again, this phenomenon can be attributed to the large real surface of the nanotubes and consequently, the larger area for polymer-grafting.

The surface modification after grafting was verified by the change in the wettability of the samples using infrared spectrum of the surfaces and contact angle measured using the sessile drop method. The values were compared with those obtained for groups A and B. Fig. 4 shows the contact angle values for the evaluated groups.

All surfaces show hydrophilic behavior, the surface of the group A had a higher value of contact angle (72°), followed by the group C (43°) and B (4°). The change of contact angle verified in the grafted sample confirms the efficiency of the process and supports the findings of Ben Aissa et al. [21] and Vasconcelos et al. [23]. This change can be attributed mainly to the change in surface chemistry effected by insertion of polar groups in the grafted polymer. However, superhydrophilic surfaces were obtained after TiO_2 nanotubes growth and this result is in accordance with our previous studies [29–31].

The chemical composition of the group C was evaluated using FTIR. The Fig. 5 shows the spectra after PNaSS UV grafting. The results confirm surface modification by the presence of several characteristic peaks of PNaSS, especially the double peak 1010/1040 cm^{-1} representing the aromatic ring and the O═S═O group present in the NaSS structure [17,26]. The peak in the region of 1650 cm^{-1} was also verified by Felgueiras et al. [2] and can be related to the C═C bond of the aromatic ring. For this same structure, but for C═H bonds peaks can be observed at 990 and 2950 cm^{-1}. Finally, the peak at 1180 cm^{-1}

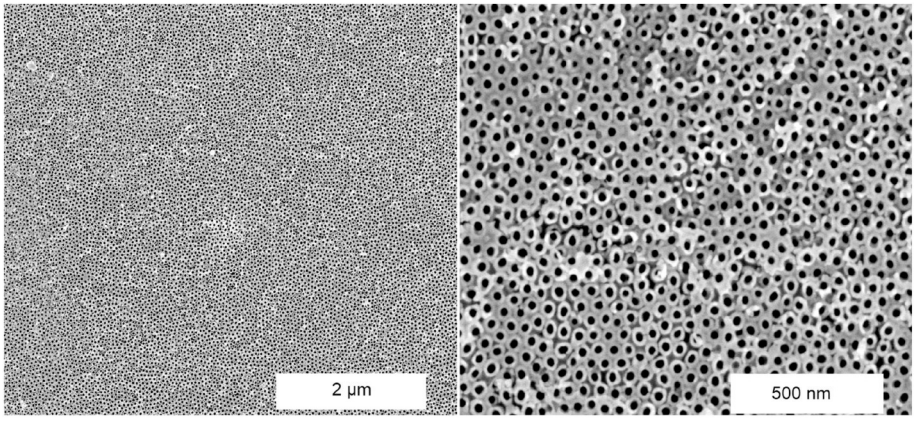

Fig. 2. SEM images of Ti15Mo alloy surface after anodization (top view) containing TiO_2 nanotubes formed in ammonium fluoride/glycerol electrolyte (a) overview and (b) nanotubes details.

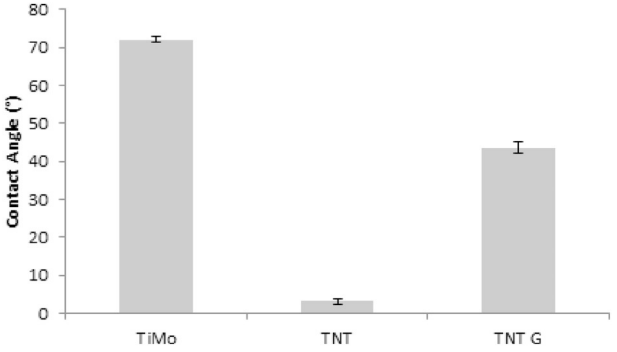

Fig. 4. Contact angle by the sessile drop method for flat samples (group A), anodized and non-grafted (group B) and anodized and grafted (group C) samples.

is representative of SO_3^- groups and it was also found by Chouirfa et al. [25] in their work on PNaSS grafting.

3.2. Cells culture

The early adhesion rate and adhesion after sheer stress of osteoblasts were studied after 15 min of incubation. The results are expressed as adhesion percentage before and after stress application, as shown in Fig. 6.

After 15 min of incubation at least 20% of the cells were already adhered to the surfaces. Analysis of variance ($p = 0.05$) shows that group C values can be considered as statistically superior to the others with over 40% of the cells already adhered. The improvement of cell adhesion on surfaces rich in sulfonate groups has already been reported in fibroblasts by Kowalczyńska et al. [32], allowing the conclusion that short-term adhesion is mainly driven by surface chemistry. As a matter of fact, the surface composition induces a particular conformation of adsorbed proteins [33]. In the presence of PNaSS, sites favorable to cell attachment will be more exposed to integrin biding, especially by FAK pathway [34]. This rapid interaction and consequent cell adhesion is primordial to the success of a prosthesis [34,35] since *in vivo* the osseous cells will compete with other cells, especially with connective tissue cells which once installed will create a tissue fibrosis, preventing the adhesion of osseous cells and subsequent osteointegration [36].

In order to evaluate the strength of cell adhesion, the initial interaction between the osteoblasts and the surfaces were evaluated after shear stress for 15 min. Both group A and C samples showed more than 60% cells after stress test. These values can be considered relatively high values for cells interacting with the surfaces for only 15 min before the application of the load. Among the different studied surfaces, the group B is the only one considered to be statistically superior to the

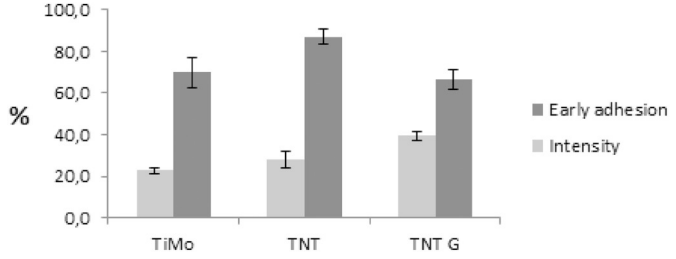

Fig. 6. Percentage of adhered cells after 15 min of incubation and after shear stress for flat samples (group A), anodized and non-grafted (group B) and anodized and grafted samples (group C).

others ($p = 0.05$), which may indicate that, contrary to what was verified in the initial adhesion percentage, this parameter is governed mainly by morphology of the surface and not by its chemical composition.

The images after day 1 of cell culture allow distinguishing some important points about the influence of the surface characteristics on the cellular growth. Fig. 7 shows a view of the cell morphology on the evaluated surfaces. For group A, elongated cells were observed. As shown by Das et al. [11], cells on non-anodized surfaces have an elongated and flattened shape compared to the more polygonal shape found on surfaces with nanotubes. The main cause of this difference is the cytoplasmic volume, which in the case of the group A is reduced and tends to grow in the grooves created by the surface preparation, different from what happens to group B where the cytoplasm distributes radially forming a confluence of cells (Fig. 7b).

Although in samples of the group C (Fig. 7c) the polygonal shape remains, the volume of the extracellular matrix is visibly larger, which could be confirmed when using ImageJ software to quantify the covered surface in each studied group. Three different zones of each sample were used for this quantification and it was found that grafted samples were significantly ($p = 0.01$) more covered than the other (Fig. 8). Such an increase was reported in the literature [21] and can be associated with facilitated binding between cell proteins and PNaSS.

Cell viability and cytotoxicity were evaluated after 24 h of culture by MTT assay. The absorbance translates the rate of tetrazolium salt reduction into formazan crystals by mitochondrial activity. The values were compared to a curve of absorbance of known cells concentrations. The percentage of viable cells can be seen in Fig. 9.

Although all surfaces revealed more than 70% of viable cells and can be therefore considered as non-cytotoxic, the value found for group C was significantly ($p = 0.01$) higher than that of group B, confirming the beneficial effect of PNaSS on the osteoblast cell response.

From this point, the osteoblasts proliferation was studied for 1, 3 and 7 days of culture. In Fig. 10, the evolution of the cells numbers over

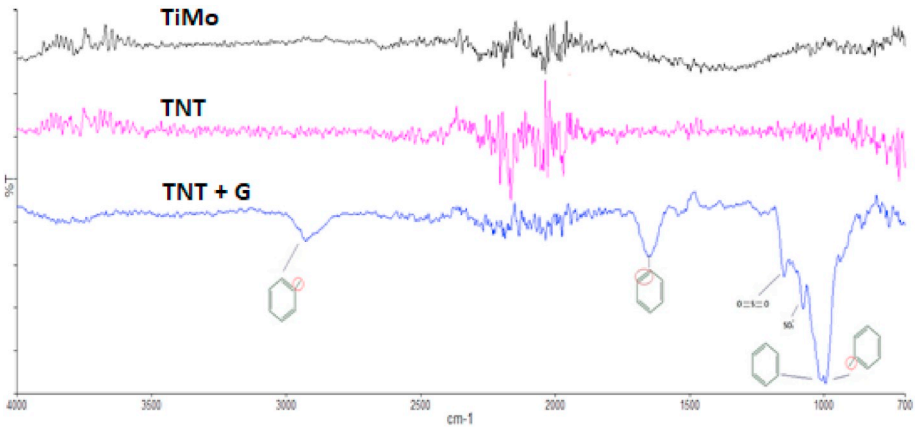

Fig. 5. FTIR spectrum of TiMo alloy, anodized and grafted surface. The defining main peaks for pNaSS presence are highlighted in the grafted spectrum (TNT + G).

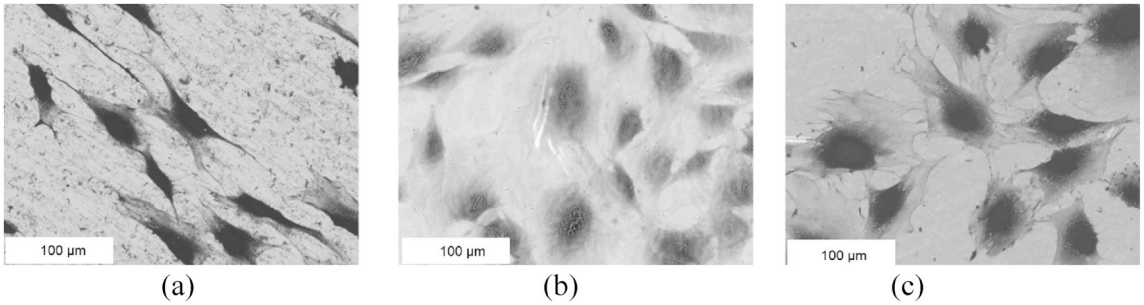

Fig. 7. SEM images of osteoblast after 24 h on the surface: a) Ti15Mo flat samples, b) Ti15Mo anodized samples and c) Ti15Mo anodized and grafted surfaces.

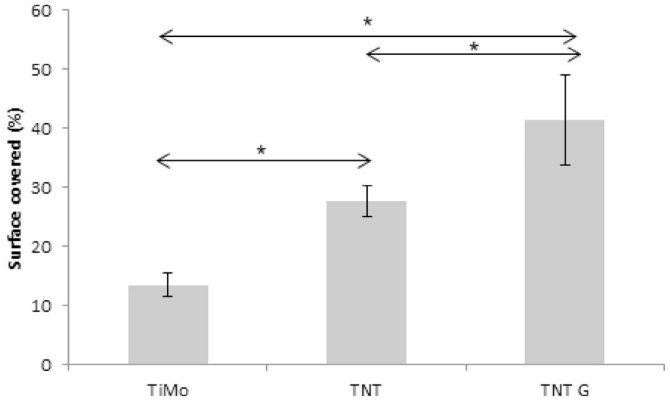

Fig. 8. Mean percentage of as received (group A), anodized (group B) and PNaSS grafted surfaces (group C) covered by osteoblasts after 24 h incubation.

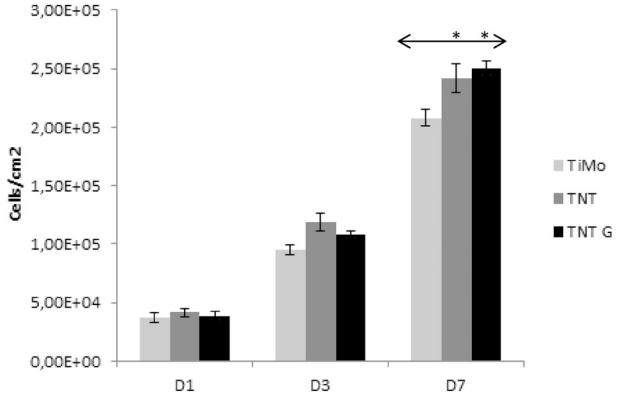

Fig. 10. Cells per cm^2 of PNaSS grafted (group C), and non-grafted nanotubes (group B), as well as flat Ti15Mo alloys (group A) as control group.

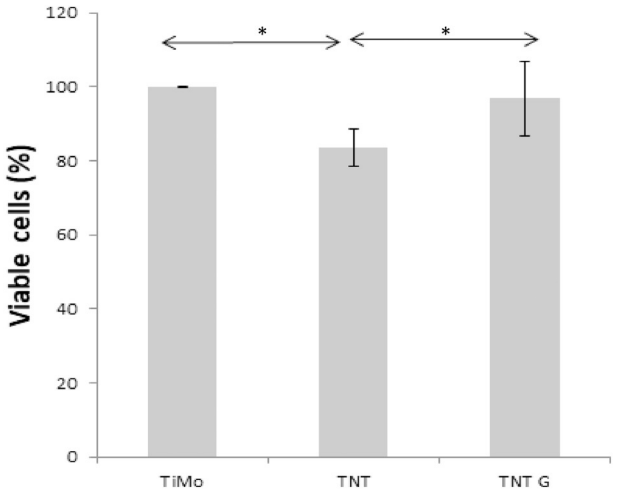

Fig. 9. Percentage of viable osteoblasts over titanium alloy, nanotubes and grafted titanium nanotubes after 24 h incubation.

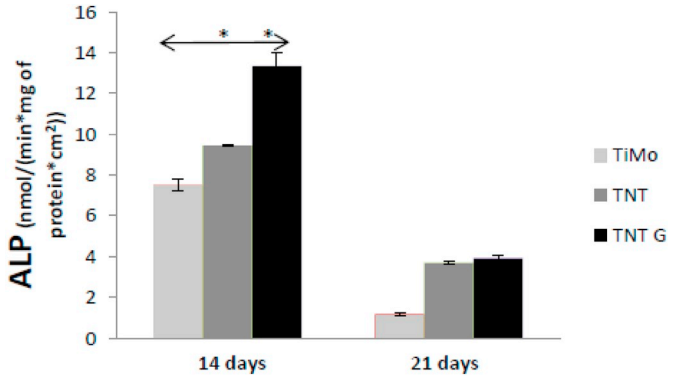

Fig. 11. Conversion of *p*-nitropenol by the action of the enzyme ALP at the surfaces of different groups studied: flat samples (group A), anodized (group B) and PNaSS grafted surfaces (group C).

the surfaces can be observed.

At day 1, no significant difference was noticed between groups. At day 3, samples of group B exhibit the higher values while at day 7 surfaces of groups B and C were significantly ($p = 0.05$) more populated.

The superior proliferation of the MC3T3-E1 lineage on nanostructured surfaces compared to its polished analogues has already been reported for titanium samples [4] and confirms the hypothesis that the combination of anchoring friendly structure and reduced contact angle of nanotubes has a favorable effect on *in vitro* cell cultures. The superiority of the group C can be also related to the surface chemistry, especially the presence of SO_3^- groups, which creates conditions for the connection between cells and the surface in the presence of proteins, as reported by Felgueiras et al. [2].

The activity of the alkaline phosphatase enzyme acts as the primary indicator of the *in vitro* differentiation and it was evaluated after 14 and 21 days of culture. The results are shown in Fig. 11.

The alkaline phosphatase enzyme activity (ALP) was statistically higher ($p = 0.05$) for samples of group B than for group A after 14 and 21 days of culture. This result confirms the tendency found in several studies that the osteoblastic differentiation is favored by anodized surfaces [4,11,37]. The enzymatic activity after 14 days is also significantly higher in group C than in any other studied group, once again this increase has been documented in the literature [18,25] confirming the influence of NaSS on the binding between treated surfaces and extra cellular matrix proteins, especially collagen one of the prominent extracellular matrix formers during cell differentiation. The smaller values at 21 days of incubation can be interpreted as maturation of the extracellular matrix [2,17] and progress of the differentiation process

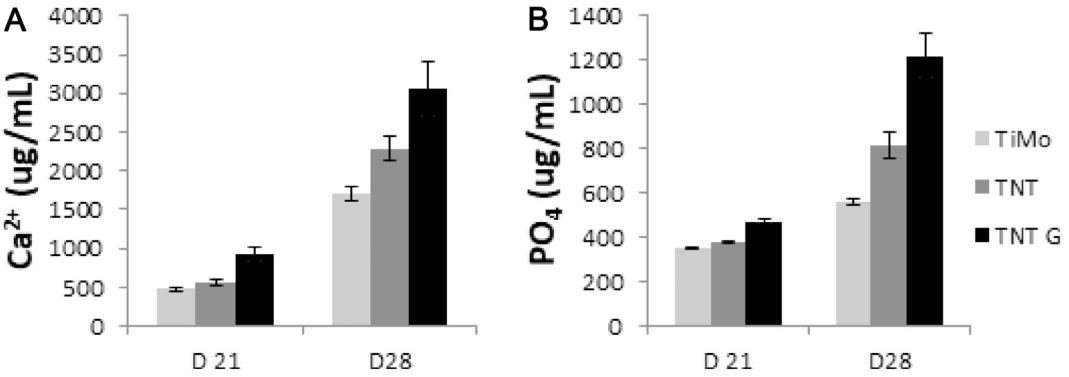

Fig. 12. Production of A) calcium and B) phosphate by osteoblasts after 3 and 4 weeks of incubation on different surfaces.

since ALP activity is decreased in detriment of the deposition of calcium and phosphate in the second stage of differentiation.

To confirm this statement, surfaces were evaluated after 21 and 28 days of culture and the results are shown in Fig. 12.

As expected, given the ALP results, surfaces of the group C present statistically superior mineralization than the other surface groups for both markers ($p < 0.05$). The difference is even more prominent after 28 days, indicating larger osteoblast maturation. Such results once again can be correlated to the influence of the SO_3^- groups on the specific adsorption of extracellular matrix proteins [18,19,21,26].

3.3. Bacterial colonization

The antimicrobial activity of the coated samples was evaluated against *S. aureus* (ATCC 25924) and *C. albicans* (SC 5314) microorganisms in mature mixed biofilms of 48 h.

The Fig. 13 revealed a homogeneous accumulation of *C. albicans* (hyphae-shaped) and *S. aureus* (cocci-shaped) as a dual-species biofilm after 48 h of culture on group A specimens. Moreover, according to the literature [38,39] surfaces containing TiO_2 nanotubes reduce the bacterial adhesion, which could be verified in this study, since samples of the group B, showed a decrease in *S. aureus* presence. However the *C. albicans* presence seems to be amplified, this phenomenon can be related to higher roughness and available surface area of anodized samples, and it was verified in different surfaces [40,41]. In addition, samples of the group C showed a beneficial effect and a significant decrease in both microorganisms' adhesion and *C. albicans* viability. This result confirms the low adhesion of bacteria to PNaSS grafted

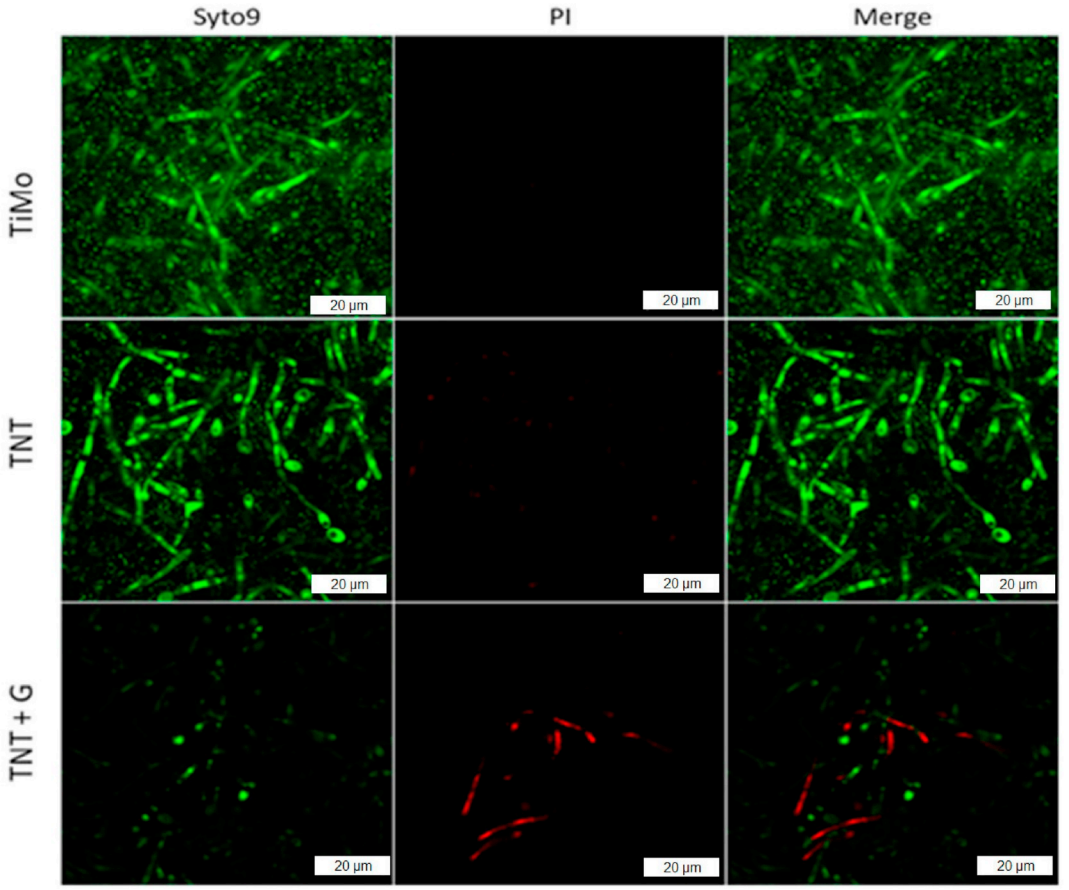

Fig. 13. Confocal Laser Scanning Microscope (CLSM) images of live/dead staining at 48 h. Cell types viable are visualized by green fluorescent staining (Syto 9) and dead bacteria by red fluorescence (Propidium Iodide). (For interpretation of the references to color in this figure legend, the reader is referred to the web version of this article.)

surfaces [21,23] due to the proteins arrangement and conformation over the treated surface. Furthermore, the reduction of *S. aureus* adhesion and presence may exert an influence on the formation of the biofilm [17] and consequently reduce the existence of *C. albicans*.

4. Conclusion

In summary, this study assessed the effect of successive surfaces modifications of a beta-titanium alloy and their influence on cell response (adhesion to differentiation) and bacterial adhesion. The nanotubes morphology was stable and homogeneous over the sample surface and the surfaces showed an encouraging PNaSS grafting degree. Cell behavior changed for both treatments in every investigated assay, from early adhesion to osteoblastic differentiation. PNaSS grafted samples showed significantly better interaction with osteoblast cells which can be related to an enhanced interaction between cells and the surface due the presence of sulfonate groups. In addition, the presence of PNaSS grafting reduced bacteria adhesion and fungal activity.

Author contributions

André L. R. Rangel: Investigation, Formal analysis, Writing - Original Draft, Writing - Review & Editing.

Céline Falentin-Daudré: Conceptualization, Methodology.

Bruna Natália Alves da Silva Pimentel: Investigation.

Carlos Eduardo Vergani: Methodology, Formal analysis.

Véronique Migonney: Conceptualization, Methodology, Validation, Supervision, Writing - Review & Editing.

Ana P. R. Alves Claro: Conceptualization, Methodology, Validation, Supervision, Writing - Review & Editing, Funding acquisition.

Acknowledgment

The authors would like to thank FAPESP (projects 2013/00317-4, 2015/26273-9, 2015/25124-0 and 2015/13834-2) and CNPq (project 486352-2013-7) for their financial support.

Appendix A

Cell culture essais

Surface and cell preparation

Prior to the tests the surfaces were washed for conditioning. The process consists of 3 washes of 3 h in 1.5 mol/l NaCl solution, 0.15 mol/l NaCl and phosphate-buffered saline (PBS), between each solution the samples were washed for 10 min in ultra-pure water. For sterilization the samples were rinsed in ethanol (70% in water) for 20 min and exposed to a UV germicidal lamp of a tissue culture hood for 15 min each side. The samples were then transferred to well-plates containing α-MEM cells culture media and kept overnight. Finally, the samples were transferred to wells containing enriched α-MEM media (1% penicillin, 1% glutamine, 10% fetal bovine serum) and stored until the beginning of the assays. This study was performed using osteoblasts of MC3T3-E1 (subclone 4 ATCC) lineage passages 2–6, stored in a −80 °C freezer and thawed in a 37 °C water bath prior to the procedure. All assays were performed in triplicate in a laminar flow chamber under sterile conditions. Quantitative results were evaluated by analysis of variances (ANOVA).

Cell adhesion

For the short-term cell adhesion and adhesion strength test, samples were distributed in a 24-well plate and seeded in 1 ml of cell suspension (50,000 cells/ml) for 15 min. After that period, each well was cleared, the suspensions recovered separately (N1) and stored at 37 °C. Samples were then repositioned in the center of the 24 well-plate containing 1 ml of α-MEM in each well and subjected to controlled rotation in order to create a shear stress of 10 dyn/cm^2 on the surface for 15 min. The medium recovered after stress application was also recovered and stored at 37 °C (N2). Finally, the samples were transferred to new wells washed in pbs and immersed in 1 ml of trypsin to separate the adherent cells. The action of the trypsin was stopped by the addition of 1 ml of enriched α-MEM and the resulting suspensions also stored (N3). The number of cells in each step of the assay (N1, N2 and N3) was measured by particle counting. The value of N1 represents the number of cells not adhered in short-term, the value N2 represents the number of cells separated by the applied stress and N3 the number of cells adhered after stress. Short-term adhesion is given by the following formula:

$$\%A15 = (N2 + N3)/(N1+N2+N3).$$

Similarly, the intensity of adhesion between cells and the surface can be indirectly measured by the percentage of cells adhered to at the end of the experiment:

$$\%A = N3/(N2 + N3).$$

Cell viability

24 h after the seeding, the samples were washed twice in PBS and transferred to a 24-well plate with 1 ml of PBS per well over which 50 μl of 5 mg/ml MTT solution (3-(4,5-dimethylthiazolyl-2)-2,5-diphenyltetrazolium bromide) in PBS was added. The samples were incubated for 4 h (37 °C and 5% CO_2). After incubation the wells were emptied and the formazan crystals dissolved by addition of 1 ml of dimethylsulfoxide (DMSO) under mechanical stirring for 10 min. The absorbance of the solution was measured using an UV–vis reader (PerkinElmer lambda 25).

Cell proliferation

For each evaluated time point the samples were taken from the culture medium and washed in PBS twice before being transferred to a new well. 1 ml of trypsin was added to each well for enzymatic digestion for 7 min at 37 °C. The action of trypsin was stopped by addition of 1 ml of enriched α-MEM and the amount of cells recovered was analyzed by counting the particles between 10 and 60 μm in diameter.

Cell differentiation

For differentiation essays the enriched α-MEM media was modified with addition of 0.05 mM L-ascorbic acid and 10 mM and β-glycerophosphate to ensure cells maturation. To measure alkaline phosphatase activity, after 14 and 21 days of culture the samples were washed twice in PBS and transferred to a new well containing 1 ml of triz-Triton ×100 buffer solution. The samples were shaken for 1 h and the resulting suspensions were

transferred to test tubes, frozen at −80 °C and thawed at 37 °C. After repeating the procedure 3 times 500 μl of suspension from each tube were mixed with 500 μl of 20 mM *p*-nitrophenyl phosphate solution and incubated for 30 min at 37 °C. The absorbance of the solution is measured by UV–vis spectrophotometry at 405 nm (PerkinElmer lambda 25). The amount of ALP produced was normalized by the total concentration of proteins in the suspension, measured with the aid of the commercial Bio-Rad protein assay kit.

For mineralization calcium and phosphate deposits were evaluated after 21 and 28 days of culture. The samples were initially washed twice in PBS, transferred to a new well containing 1 ml of 15% (w/v) trichloroacetic acid solution and shaken for 1 h at room temperature. 10 μL of each well was added to 1 ml of arsenazo III solution (0.2 mM in PBS) and held for 15 min. The amount of calcium present can be determined by absorption at 650 nm against a curve of known Ca^{2+} concentrations. For evaluation of the amount of phosphate, the remainders of the suspensions were kept under stirring for a further 48 h. 100 μl of these suspensions were added to 400 μl of acetone, 200 μl of sulfuric acid 2.5 M, 200 μl of ammonia molybdate 10 mM and 80 μl of l citric acid 1 M. The resulting suspension was stirred vigorously and incubated for 30 min. The phosphate concentration can be assessed by absorption at 355 nm against a known PO_4^- concentration curve. Both absorptions were measured by UV–vis spectroscopy (PerkinElmer lambda 25).

Bacterial colonization assay

Standard strains of the bacterium *Staphylococcus aureus* (ATCC 25923) and *Candida albicans* (SC 5314) were used for this study. The bacterium was seeded in Miller Hinton Agar (MHA) and incubated at 37 °C for 48 h. Then, eight colonies were transferred to 10 ml of Tryptic Soy Broth culture medium (TSB), the pre-inoculum and incubated overnight at 37 °C. After that time, 1.5 ml of the pre-inoculum were transferred to a new falcon tube containing 28.5 ml of fresh TSB medium forming the inoculum, and incubated for 4 h at 37 °C. The optical density of the inoculum (OD 600 nm) was then checked for standardization. In parallel, the fungus was sown in Sabouraud Dextrose Agar (SDA) and incubated at 37 °C for 48 h. Then, five colonies were transferred to 10 ml of Yeast Nitrogen Base (YNB) medium forming the pre-inoculum, and incubated overnight at 37 °C. 3 ml of the pre-inoculum were transferred to a new falcon tube containing 27 ml of fresh YNB and incubated for 8 h at 37 °C. The optical density of the inoculum (OD 540 nm) was also checked for standardization. Suspensions of microorganisms were centrifuged (4000 $\times g$ for 5 min at 4 °C) and the pellets washed with PBS (pH 7.0). Further centrifugation was performed so that the pellets were re-suspended in HEPES-buffered RPMI culture medium (pH 7.0).

Samples were packed into a 24-well plate, and 1 ml of each inoculum was added to each well. For the microorganisms to adhere, the plate was incubated with orbital shaker (37 °C, 75 rpm) for 90 min. After this period two washes were performed with 1 ml PBS for the removal of the non-adhered microorganisms. Two milliliters of HEPES buffered RPMI medium was then added to each well, and the plate was incubated with orbital shaker for 48 h, with medium exchange after 24 h.

Before imaging, the samples were stained with propidium iodide and syto 9 (LIVE/DEAD BacLight Bacterial Viability Kit, Life Technology, ThermoFischer, Waltham, MA, USA). Fluorophores were prepared according to the manufacturer's instructions and kept in contact with the specimens for 15 min in a dark environment. After that period, the specimens were transferred to confocal petri dishes (Confocal Dishes [200350], SPL Life Sciences, Korea) and taken for analysis by laser confocal microscope (Carl Zeiss LSM 800 with Airyscan, Zeiss, Germany). The images were obtained in two channels (488 nm and 561 nm) and with a 63× objective. After the acquisition of the images, they were analyzed with the help of the software ZEN Blue 2.3 system (Carl Zeiss, Germany).

References

[1] S. Lavenus, J. Ricquier, G. Louarn, P. Layrolle, Cell interaction with nanopatterned surface of implants, Nanomedicine 5 (6) (2010).

[2] H.P. Felgueiras, M. Evans, V. Migonney, Contribution of fibronectin and vitronectin to the adhesion and morphology of MC3T3-E1 osteoblastic cells to poly(NaSS) grafted Ti6Al4V, Acta Biomater. 28 (2015) 225–233.

[3] K.C. Popat, M. Eltgroth, T.J. Latempa, C.A. Grimes, T.A. Desai, Decreased Staphylococcus epidermis adhesion and increased osteoblast functionality on antibiotic-loaded titania nanotubes, Biomaterials 28 (32) (2007) 4880–4888.

[4] K.C. Popat, L. Leoni, C.A. Grimes, T.A. Desai, Influence of engineered titania nanotubular surfaces on bone cells, Biomaterials 28 (21) (2007) 3188–3197.

[5] B.S. Smith, S. Yoriya, L. Grissom, C.A. Grimes, K.C. Popat, Hemocompatibility of titania nanotube arrays, J. Biomed. Mater. Res. A 95A (2) (2010) 350–360.

[6] B.S. Smith, S. Yoriya, T. Johnson, K.C. Popat, Dermal fibroblast and epidermal keratinocyte functionality on titania nanotube arrays, Acta Biomater. 7 (6) (2011) 2686–2696.

[7] S. Bauer, A. Pittrof, H. Tsuchiya, P. Schmuki, Size-effects in TiO_2 nanotubes: diameter dependent anatase/rutile stabilization, Electrochem. Commun. 13 (6) (2011) 538–541.

[8] A.L.R. Rangel, G.R. Moreira Santos, A.P.R. Alves Claro, Nanotubes growth on Ti-15Mo alloys by anodization at low voltage, Mater. Sci. Forum 869 (2016) 924–929.

[9] K.S. Brammer, S. Oh, C. Cobb, L. Bjursten, H. van der Heyde, S. Jin, Improved bone-forming functionality on diameter-controlled TiO2 nanotube surface, Acta Biomater. 5 (8) (2009) 3215–3223.

[10] S. Oh, C. Daraio, L.H. Chen, T.R. Pisanic, R.R. Fiñones, S. Jin, Significantly accelerated osteoblast cell growth on aligned TiO2 nanotubes, J. Biomed. Mater. Res. A 78 (1) (Jul 2006) 97–103.

[11] K. Das, S. Bose, A. Bandyopadhyay, TiO2 nanotubes on Ti: influence of nanoscale morphology on bone cell–materials interaction, J. Biomed. Mater. Res. A 90 (1) (2009) 225–237.

[12] S. Saidin, P. Chevallier, M.R. Abdul Kadir, H. Hermawan, D. Mantovani, Polydopamine as an intermediate layer for silver and hydroxyapatite immobilisation on metallic biomaterials surface, Mater. Sci. Eng. C 33 (8) (2013) 4715–4724.

[13] M. Lai, K. Cai, L. Zhao, X. Chen, Y. Hou, Z. Yang, Surface functionalization of TiO 2 nanotubes with bone morphogenetic protein 2 and its synergistic effect on the differentiation of mesenchymal stem cells, Biomacromolecules 12 (2011) 1097–1105.

[14] G. Zorn, J. Baio, T. Weidner, Migonney, V. Migonney, D. Castner, Characterization of poly(sodium styrene sulfonate) thin films grafted from functionalized titanium surfaces, Langmuir 27 (2011) 13104–13112 (American Chemical Society).

[15] V. Migonney, I. Ben Aissa, D. Lutomski, G. Hélary, S. Oughlis, F. Poirier, S. Changotade, J. Peltzer, J. Lataillade, D. Blanquaert, B. de Lambert, V. Viateau, M. Manassero, A. Crémieux, A. Saleh-Mghir, D. Thomas, Controlled cell adhesion and activity onto TAl6V titanium alloy by grafting of the surface: elaboration of orthopaedic implants capable of preventing joint prosthesis infection, IRBM 34 (2) (2013) 180–185.

[16] S. Oughlis, S. Lessim, S. Changotade, F. Bollotte, F. Poirier F, G. Hélary, J. Lataillade, V. Migonney, D. Lutomski, Development of proteomic tools to study protein adsorption on a biomaterial, titanium grafted with poly(sodium styrene sulfonate), J. Chromatogr. B Anal. Technol. Biomed. Life Sci. 879 (31) (2011) 3681–3687.

[17] A. Alcheikh, G. Pavon-Djavid, G. Helary, H. Petite, V. Migonney, F. Anagnostou, PolyNaSS grafting on titanium surfaces enhances osteoblast differentiation and inhibits Staphylococcus aureus adhesion, J. Mater. Sci. Mater. Med. 24 (2013) 1745–1754.

[18] J. Mayingi, G. Hélary, F. Noirclere, B. Bacroix, V. Migonney, Synthèse et greffage de polymères bioactifs sur des surfaces en titane pour favoriser l'ostéointégration Grafting of bioactive polymers onto titanium surfaces and human osteoblasts response, ITBM-RBM 29 (2008) 1–6.

[19] S. Kerner, V. Migonney, G. Pavon-Djavid, G. Helary, L. Sedel, F. Anagnostou, Bone tissue response to titanium implant surfaces modified with carboxylate and sulfonate groups, J. Mater. Sci. Mater. Med. 21 (2010) 707–715.

[20] H. Felgueiras, A. Decambron, M. Manassero, L. Tulasne, M. Evans, V. Viateau, V. Migonney, Bone tissue response induced by bioactive polymer functionalized Ti6Al4V surfaces: in vitro and in vivo study, J. Colloid Interface Sci. 491 (2017) 44–54.

[21] I. Ben Aissa, G. Helary, V. Migonney, Le greffage radicalaire de polymères bioactifs sur le titane pour prèvenir l'infection sur prothèse articulaire, IRBM 32 (5) (2011) 322–325.

[22] J. Zhou, G. Pavon-Djavid, F. Anagnostou, V. Migonney, Inhibition de l'adhérence de Porphyromonas gingivalis sur la surface de titane greffé de poly(styrène sulfonate de sodium), IRBM 28 (1) (2007) 42–48.

[23] D. Vasconcelos, C. Falentin-Daudré, D. Blanquaert, D. Thomas, P. Granja, V. Migonney, Role of protein environment and bioactive polymer grafting in the S. epidermidis response to titanium alloy for biomedical applications, Mater. Sci. Eng. C 45 (2014) 176–183.

[24] C. Falentin-Daudré, V. Migonney, H. Chouirfa, J.S. Baumann, Procédé de greffage de polymères bioactifs sur des matériaux métalliques, (2015) (Brevet B248515D34589).
[25] L.V. Taveira, J.M. Macák, H. Tsuchiya, L.F.P. Dick, P. Schmuki, Initiation and growth of self-organized TiO_2 nanotubes anodically formed in $NH_4F/(NH_4)_2SO_4$ electrolytes, J. Electrochem. Soc. 152 (10) (2005) B405–B410.
[26] H. Chouirfa, V. Migonney, C. Falentin-Daudré, Grafting bioactive polymers onto titanium implants by UV irradiation, RSC Adv. 6 (2016) 13766–13771.
[27] G. Helary, F. Noirclere, J. Mayingi, V. Migonney, A new approach to graft bioactive polymer on titanium implants: improvement of MG 63 cell differentiation onto this coating, Acta Biomater. 5 (2009) 124–133.
[28] J. Chaves, A.L.A. Escada, A. Rodrigues, A.P.R. Alves Claro, Characterization of the structure, thermal stability and wettability of the TiO_2 nanotubes growth on the Ti-7.5Mo alloy surface, Appl. Surf. Sci. 370 (2016) 76–82.
[29] P. Capellato, B. Smith, K. Popat, A.P.R. Alves Claro, Fibroblast functionality on novel Ti-30Ta nanotube array, Mater. Sci. Eng. C 32 (2012) 2060 (Biomimetic Materials, Sensors and Systems, Materials Science and Engineering C).
[30] A.L.A. Escada, R.Z. Nakazato, A.P.R. Alves Claro, Growth of TiO_2 nanotubes by anodization of Ti–7.5Mo in NH_4F solutions, Nanosci. Nanotechnol. Lett. 5 (4) (2013) 510–512 [S.l.].
[31] A.L.A. Escada, N. Trujillo, K. Popat, A.P.R. Alves Claro, Human dermal fibroblast adhesion on Ti-7.5Mo after TiO_2 nanotubes growth, Mater. Sci. Forum 889 (2017) 195–200.
[32] H. Kowalczyńska, M. Nowak-Wyrzykowska, Modulation of adhesion, spreading and cytoskeleton organization of 3T3 fibroblasts by sulfonic groups present on polymer surfaces, Cell Biol. Int. 27 (2) (2003) 101–114.
[33] C. Latz, G. Pavon-Djavid, G. Helary, M. Evans, V. Migonney, Alternative intracellular signaling mechanism involved in the inhibitory biological response of functionalized PMMA-based polymers, Biomacromolecules 4 (2003) 766–771.
[34] H. Felgueiras, V. Migonney, Sulfonate groups grafted on Ti6Al4V favor MC3T3-E1 cell performance in serum free medium conditions, Mater. Sci. Eng. C 39 (2014) 196–202.
[35] K. Brammer, C. Frandsen, S. Jin, TiO_2 nanotubes for bone regeneration, Trends Biotechnol. 30 (6) (2012) 315–322.
[36] R. Wang, Y. Li, In vitro evaluation of biocompatibility of experimental titanium alloys for dental restorations, J. Prosthet. Dent. 80 (4) (1998) 495–500.
[37] S.H. Oh, S. Jin, Titanium oxide nanotubes with controlled morphology for enhanced bone growth, Mater. Sci. Eng. C 26 (2006) 1301–1306.
[38] C. Yao, E.B. Slamovich, T.J. Webster, Enhanced osteoblast functions on anodized titanium with nanotube-like structures, J. Biomed. Mater. Res. A 85 (1) (2008) 157–166.
[39] B. Ercan, E. Taylor, E. Alpaslan, T.J. Webster, Diameter of titanium nanotubes influences anti-bacterial efficacy, Nanotechnology Jun 15;22 (29) (2011) 295102.
[40] J. Verran, C.J. Maryan, Retention of Candida albicans on acrylic resin and silicone of different surface topography, J. Prosthet. Dent. 77 (5) (May 1997) 535–539.
[41] C.S. Tsang, H. Ng, A.S. McMillan, Antifungal susceptibility of Candida albicans biofilms on titanium discs with different surface roughness, Clin. Oral Investig. 11 (4) (2007) 361–368 Dec.